Nonreciprocal transmission in a cavity-magnon system by rotational Sagnac effect

Zhe-Qi Yang, Si-Qi Lin, and Zhi-Rong Zhong*

Fujian Key Laboratory of Quantum Information and Quantum Optics, College of Physics and Information Engineering, Fuzhou University, Fuzhou, Fujian 350108, China

(Received 25 August 2025; accepted 6 November 2025; published 8 December 2025)

Ultrahigh nonreciprocal transmission has been achieved in a cavity-magnon system, which consists of two whispering gallery modes (WGMs) and a single magnon mode within a magnetic insulator yttrium iron garnet sphere. The nonreciprocal frequency shift induced by the Sagnac effect enables unidirectional transmission of an input field, while suppressing propagation in the opposite direction, thereby facilitating nonreciprocal optical transmission. Within experimentally accessible parameter regimes, the optical isolation ratio can exceed 40 dB, representing the highest isolation ratio reported to date. Furthermore, applying squeezing to the magnon mode further enhances this isolation performance. Additionally, the directionality of light isolation can be reversed simply by modifying the rotation of the WGM cavity. These findings offer promising prospects for developing high-performance, tunable, and compact optical nonreciprocal devices.

DOI: 10.1103/27cz-jqd4

I. INTRODUCTION

Nonreciprocal light propagation, which describes the asymmetric transmission of optical signals between forward and backward directions, plays a critical role in sensitive signal processing and detection, particularly within the precise context of quantum systems [1–4]. In stark contrast to reciprocal systems governed by Lorentz reciprocity, nonreciprocal devices break time-reversal symmetry [5], enabling critical functionalities such as optical isolation, unidirectional amplification, and magnetic-free circulators [6–9]. Conventional nonreciprocal devices typically achieve time-reversal symmetry breaking by employing ferromagnetic compounds and leveraging the Faraday effect in conjunction with strong magnetic fields [10–12], angular momentum biasing in photonic or acoustic crystals [13–15], nonlinear spatiotemporal modulation [16–18], and optomechanical coupling [19–24]. However, the bulkiness and high cost of ferrite-based systems impede the miniaturization and integration of nonreciprocal devices. Thanks to advances and maturation in micro/nanofabrication techniques, compact and highly tunable cavity-magnon systems provide an attractive platform for achieving nonreciprocal optical transmission.

Magnons, the quantized spin wave excitations associated with spin ordering in magnets, have attracted significant interest across various fields of physics [25–33], such as magnon Kerr effect [34,35], magnon polaritons [36–40], and non-Hermitian physics [33,41,42]. Notably, due to their precisely tunable magnon frequency and coupling strength, long coherence times, and low dissipation [43–49], cavity-magnon systems have great potential for applications in the field of quantum technology [50], for example, quantum sensing [51–53], quantum transducers [54–56], quantum memory [57,58], etc. In recent years, cavity-magnon systems have been increasingly explored for achieving nonreciprocal transmission via various approaches [59–64]. However, current approaches to nonreciprocal optical transmission often face challenges such as low isolation ratios and transmission efficiencies, leading to systems with reduced performance, decreased reliability, and increased susceptibility to interference. For example, in Ref. [59], nonreciprocal transmission has been achieved by utilizing the magnon Kerr nonlinearity, reaching a maximum isolation ratio of 21 dB with a forward transmission coefficient of 0.06. In another work, Ref. [61] has demonstrated nonreciprocity through quantum interference between different transmission paths in a three-mode cavity magnonics system, attaining a maximum isolation of 34 dB and a forward transmission coefficient of 0.13. Therefore, developing a method to enhance nonreciprocal transmission isolation while maintaining flexibility and ease of control remains a significant challenge.

In the present work, we propose a theoretical scheme to achieve ultrahigh nonreciprocal transmission in a cavity-magnon system by rotational Sagnac effect. In the scheme, the setup consists of two whispering gallery modes (WGMs) and a single magnon mode within a magnetic insulator yttrium iron garnet (YIG) sphere. When a WGM cavity rotates, the Sagnac effect causes its clockwise (CW) and counterclockwise (CCW) propagating modes to experience opposite Fizeau frequency shifts. This nonreciprocal frequency shift causes the input light field to be transmitted in one direction while being absorbed in the opposite direction, thereby achieving nonreciprocal optical transmission. Further analysis demonstrates that, using feasible experimental parameters, the

*Contact author: zhirz@fzu.edu.cn

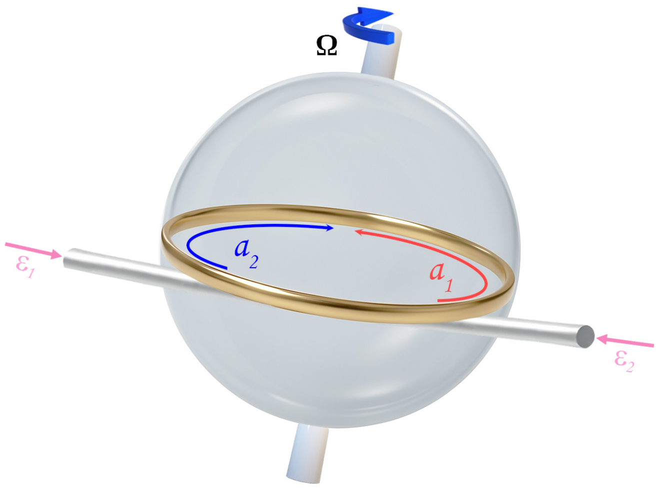

FIG. 1. Sketch of the system. A WGM cavity rotates CW with an angular velocity Ω. This cavity supports two optical modes propagating in CW and CCW directions, along with a magnetostatic mode within a YIG sphere.

system achieves an isolation ratio readily exceeding 40 dB, representing a significant improvement over previous work. Additionally, applying squeezing to the magnon mode provides an additional method for enhancement. Crucially, the direction of nonreciprocal transmission can be straightforwardly reversed by changing the WGM cavity's rotation direction, eliminating the need to adjust other system parameters and thereby offering significant practical advantages for controlling nonreciprocal transmission. Our work presents a promising avenue toward high-isolation, on-chip integrated optical nonreciprocal devices, with important implications for optical communication.

II. THEORETICAL MODEL

As illustrated in Fig. 1, we consider two optical WGMs and a magnetostatic mode supported by a YIG sphere. Coupling between the cavity mode and the magnon mode is achieved through three-wave mixing [60,65]. When a cavity rotates, the resonant frequencies of its CCW and CW propagating modes undergo a Fizeau shift [66]:

$$\Delta_F = \pm\Omega\frac{nr\omega_0}{c}\left(1-\frac{1}{n^2}-\frac{\lambda dn}{nd\lambda}\right), \tag{1}$$

where ω_0 is the resonance frequency of a nonspinning resonator. The parameter Ω is the angular velocity of the spinning resonator, n is the refractive index, r is the radius of the resonator, and $dn/d\lambda$ describes the dispersion of the medium, while c and λ represent the speed of light and the wavelength of the photon in a vacuum, respectively. When the WGM cavity rotates CW, the Fizeau shifts are $\Delta_F > 0$ for the CCW mode and $\Delta_F < 0$ for the CW mode.

The total Hamiltonian of the system can be written as ($\hbar = 1$) [60,65]

$$H = H_0 + H_{\rm int} + H_d + H_{\rm sq}, \tag{2}$$

where

$$H_0 = \sum_{j=1,2}(\omega_0+\Delta_F)a_j^\dagger a_j + \omega_m m^\dagger m, \tag{3}$$

$$H_{\rm int} = \sum_{j=1,2} g_j(a_j^\dagger m + a_j m^\dagger), \tag{4}$$

$$\begin{aligned} H_d = &\sum_{j=1,2} i\sqrt{\eta_j\kappa_j}\varepsilon_j(a_j^\dagger e^{-i\omega_{pj}t} - a_j e^{i\omega_{pj}t}) \\ &+ i\sqrt{\eta_3\gamma_m}\varepsilon_3(m^\dagger e^{-i\omega_{p3}t} - m e^{i\omega_3 t}), \end{aligned} \tag{5}$$

$$H_{\rm sq} = \frac{E}{2}(m^2 e^{i\omega_d t} + m^{\dagger 2} e^{-i\omega_d t}). \tag{6}$$

Here, H_0 is the free Hamiltonian of two WGMs and a magnon mode. a_j and $a_j^\dagger$ are the annihilation and creation operators of the cavity modes, respectively. $\Delta_F > 0$ for the a_1 mode and $\Delta_F < 0$ for the a_2 mode. The boson operators m and $m^\dagger$ represent the annihilation and creation operators for the magnon mode with frequency ω_m, which can be tuned by an external magnetic field H via $\omega_m = \gamma H$, where $\gamma/2\pi = 28$ GHz/T is the gyromagnetic ratio. $H_{\rm int}$ represents the interaction between the cavity modes and the magnon mode, where g_j is the coupling strength. H_d is the laser-driven term, with an amplitude $\varepsilon_j = \sqrt{P_j/\hbar\omega_{pj}}$ ($j = 1, 2, 3$), where P_j and ω_{pj} are the amplitude and frequency of the input field, respectively. κ_j ($j = 1, 2$) represents the total dissipation rate of the cavity mode, which includes the intrinsic dissipation $\kappa_{j,0}$ and the external dissipation $\kappa_{j,e}$ [67]. γ_m is the total loss rate of the magnon mode. The coupling parameter $\eta_j = \kappa_{j,e}/\kappa_j$ is the ratio of external loss rate to the total loss rate, which describes the coupling between the driving field and the cavity mode. Similarly, η_3 is the magnon coupling parameter. $H_{\rm sq}$ represents magnon squeezing via parametric driving [68–72], utilizing a pump field with frequency ω_d and amplitude E.

Considering $\omega_{p1} = \omega_{p2} = \omega_{p3} = \omega_d/2$, we apply a unitary transformation $V = \exp[-i\frac{\omega_d}{2}(a_1^\dagger a_1 + a_2^\dagger a_2 + m^\dagger m)t]$ to transform the Hamiltonian H to $H_1 = V^\dagger H V + i\frac{\partial V^\dagger}{\partial t}V$. Thus, we obtain a Hamiltonian

$$\begin{aligned} H_1 = &\sum_{j=1,2}[\Delta_j a_j^\dagger a_j + g_j(a_j^\dagger m + a_j m^\dagger)] \\ &+ \sum_{j=1,2} i\sqrt{\eta_j\kappa_j}\varepsilon_j(a_j^\dagger - a_j) + i\sqrt{\eta_3\gamma_m}\varepsilon_3(m^\dagger - m) \\ &+ \frac{E}{2}(m^2 + m^{\dagger 2}) + \Delta_m m^\dagger m, \end{aligned} \tag{7}$$

where $\Delta_1 = \Delta + \Delta_F$ ($\Delta_F > 0$), $\Delta_2 = \Delta + \Delta_F$ ($\Delta_F < 0$), $\Delta = \omega_0 - \omega_d/2$, and $\Delta_m = \omega_m - \omega_d/2$. By performing a Bogoliubov transformation

$$m_s = \cosh(G)m + \sinh(G)m^\dagger \tag{8}$$

on the magnon mode and applying the rotating-wave approximation, we obtain the effective Hamiltonian

$$\begin{aligned} H_{\rm eff} = &\sum_{j=1,2}[\Delta_j a_j^\dagger a_j + g_j'(a_j^\dagger m_s + a_j m_s^\dagger)] \\ &+ \sum_{j=1,2} i\sqrt{\eta_j\kappa_j}\varepsilon_j(a_j^\dagger - a_j) + i\sqrt{\eta_3\gamma_m}\varepsilon_3'(m_s^\dagger - m_s) \\ &+ \omega_s m_s^\dagger m_s, \end{aligned} \tag{9}$$

where $G = \frac{1}{4}\ln(\frac{\Delta_m+E}{\Delta_m-E})$, $g'_j = g_j \cosh(2G)$ $(j = 1, 2)$, $\varepsilon'_3 = \varepsilon_3 e^{-G}$, and $\omega_s = \sqrt{\Delta_m^2 - E^2}$.

In the long-time limit, we consider the expectation values of the operators, i.e., their steady-state solutions. We set $A_1 = \langle a_1\rangle$, $A_2 = \langle a_2\rangle$, and $M = \langle m_s\rangle$. The quantum noise terms are neglected as their expectation values are zero. The evolution of the entire system can then be described by the quantum Langevin equations

$$\begin{aligned}
&-i\Delta_1 A_1 - ig'_1 M - \frac{\kappa_1}{2}A_1 + \sqrt{\eta_1\kappa_1}\varepsilon_1 = 0,\\
&-i\Delta_2 A_2 - ig'_2 M - \frac{\kappa_2}{2}A_2 + \sqrt{\eta_2\kappa_2}\varepsilon_2 = 0,\\
&-i\omega_s M - ig'_1 A_1 - ig'_2 A_2 - \frac{\gamma_m}{2}M + \sqrt{\eta_3\gamma_m}\varepsilon'_3 = 0.
\end{aligned} \tag{10}$$

To account for nonreciprocal effects, we consider two input conditions: driving field input from the left side of the cavity, corresponding to $\varepsilon_1 \neq 0$ and $\varepsilon_2 = 0$; and from the right side, corresponding to $\varepsilon_1 = 0$ and $\varepsilon_2 \neq 0$. In fact, we only need to analyze the nonreciprocal effect for one direction of light transmission. The effect in the reverse direction is equivalent to that obtained by reversing the rotation of the resonator.

When $\varepsilon_1 \neq 0$ and $\varepsilon_2 = 0$, the steady-state solution of Eq. (10) can be obtained as follows:

$$A_1 = \frac{F_1}{D_1} - \frac{ig'_1(D_1D_2F_3 - ig'_1D_2F_1)}{D_1\left(D_1D_2D_m + D_2{g'_1}^2 + D_1{g'_2}^2\right)}, \tag{11}$$

$$A_2 = \frac{-ig'_2(D_1F_3 - ig'_1F_1)}{D_1D_2D_m + D_2{g'_1}^2 + D_1{g'_2}^2}, \tag{12}$$

where $D_1 = i\Delta_1 + \frac{\kappa_1}{2}$, $D_2 = i\Delta_2 + \frac{\kappa_2}{2}$, $D_m = i\omega_s + \frac{\gamma_m}{2}$, $F_1 = \sqrt{\eta_1\kappa_1}\varepsilon_1$, $F_2 = \sqrt{\eta_2\kappa_2}\varepsilon_2$, and $F_3 = \sqrt{\eta_3\gamma_m}\varepsilon'_3$. Substituting Eq. (12) into the standard input-output relation, the output fields $A_{2,\text{out}}$ can be written as follows:

$$\begin{aligned}
A_{2,\text{out}} &= \sqrt{\eta_2\kappa_2}A_2\\
&= \frac{-ig'_2(D_1F_3 - ig'_1F_1)\sqrt{\eta_2\kappa_2}}{D_1D_2D_m + D_2{g'_1}^2 + D_1{g'_2}^2}.
\end{aligned} \tag{13}$$

When $\varepsilon_1 = 0$ and $\varepsilon_2 \neq 0$, using the same method, the expression for the output field $A_{1,\text{out}}$ can be obtained as

$$\begin{aligned}
A_{1,\text{out}} &= \sqrt{\eta_1\kappa_1}A_1\\
&= \frac{-ig'_1(D_2F_3 - ig'_2F_2)\sqrt{\eta_1\kappa_1}}{D_1D_2D_m + D_2{g'_1}^2 + D_1{g'_2}^2}.
\end{aligned} \tag{14}$$

Subsequently, we define T_{12} and T_{21} as the forward and backward transmission coefficients, respectively, with

$$\begin{aligned}
T_{12} &= \left|\frac{A_{1,\text{out}}}{\varepsilon_2}\right|,\\
T_{21} &= \left|\frac{A_{2,\text{out}}}{\varepsilon_1}\right|.
\end{aligned} \tag{15}$$

From Eqs. (13) and (14), it is clear that when the system parameters (i.e., g'_j, η_j, κ_j, and ε_j) are fixed, the factor influencing the efficiency of nonreciprocal transmission is the difference between D_1 and D_2. This difference, in turn, is related to the angular velocity Ω of the resonator's rotation. Therefore, by adjusting Ω, we can achieve tunable optical nonreciprocal transmission. To more intuitively assess the efficiency of the nonreciprocal transmission, we define the isolation ratio by the following expression [59,61]:

$$I = 10\left|\log_{10}\frac{|A_{1,\text{out}}|^2}{|A_{2,\text{out}}|^2}\right|. \tag{16}$$

When $A_{2,\text{out}} = A_{1,\text{out}}$, the isolation $I = 0$, corresponding to the case of reciprocal transmission. A larger value of I indicates higher nonreciprocal transmission efficiency. Therefore, we will subsequently focus on the influence of system parameters on nonreciprocal transmission.

III. NONRECIPROCAL OPTICAL TRANSMISSION

In what follows, we will examine the effect of system parameters on the efficiency of nonreciprocal transmission. For simplicity, we set $\kappa_1 = \kappa_2 = \kappa$, $g'_1 = g'_2 = g = g_0\cosh(2G)$, $\eta_1 = \eta_2 = \eta_3 = \eta$, and $\varepsilon_1 = \varepsilon_2 = \varepsilon'_3$. As Δ_F is tunable, we chiefly focus on how the nonreciprocal transmission efficiency changes with Δ_F under different system conditions. To facilitate the subsequent analysis, we define $R = |\frac{A_{1,\text{out}}}{A_{2,\text{out}}}|^2$ as the intensity ratio of the forward output field to the backward output field. Differentiating R with respect to Δ_F and setting $\frac{dR}{d(\Delta_F)} = 0$, we obtain

$$\Delta_{F_{1,2}} = \pm\sqrt{\frac{\kappa^2}{4} + \left(\Delta - g\sqrt{\frac{\kappa}{\gamma_m}}\right)^2}, \tag{17}$$

$$\begin{aligned}
R(\Delta_{F_1}) &= [R(\Delta_{F_2})]^{-1}\\
&= \frac{\sqrt{\frac{\kappa^2}{4} + \left(\Delta - g\sqrt{\frac{\kappa}{\gamma_m}}\right)^2} - \left(\Delta - g\sqrt{\frac{\kappa}{\gamma_m}}\right)}{\sqrt{\frac{\kappa^2}{4} + \left(\Delta - g\sqrt{\frac{\kappa}{\gamma_m}}\right)^2} + \left(\Delta - g\sqrt{\frac{\kappa}{\gamma_m}}\right)},
\end{aligned} \tag{18}$$

where Δ_{F_1} and Δ_{F_2} are the two points at which R exhibits an extremum. Please note that at this point, $\Delta \neq g\sqrt{\frac{\kappa}{\gamma_m}}$. We will discuss the case where $\Delta = g\sqrt{\frac{\kappa}{\gamma_m}}$ later in the text. As is evident from Eq. (16), the values $R(\Delta_{F_1})$ and $R(\Delta_{F_2})$ result in the same isolation ratio I. This implies that I is maximized to the same value at both points, Δ_{F_1} and Δ_{F_2}. It should be emphasized that, experimentally, $\Omega/2\pi$ is typically on the order of kilohertz [66]. This implies that Δ_F lie approximately within the interval (−65, 65) MHz (see Sec. IV for details). Thus, all subsequent analyses are performed within this interval. The condition $\Delta_F < 0$ in this context corresponds to the scenario of the resonator rotating in the opposite direction.

As seen in Fig. 2(a), at $\Delta_F/\gamma_m = 8.295$ and $\Delta_F/\gamma_m = -8.295$, the ratio of the two transmission coefficients is maximized, and consequently, the nonreciprocal transmission effect is most pronounced. Correspondingly, in Fig. 2(b), the isolation ratio I reaches an identical maximum value of 41.63 dB at both these points. The inset in Fig. 2(a) shows that the forward transmission coefficient reaches a high of 0.67, with the backward transmission coefficient being only 0.01. Importantly, this pronounced asymmetry in transmission is maintained stably within a specific range of Δ_F/γ_m. A similar stability is also observed for the isolation ratio, as shown in the inset of Fig. 2(b). Additionally, for $\Delta_F/\gamma_m = 0$, we find $T_{21} = T_{12}$. This condition occurs when the WGM

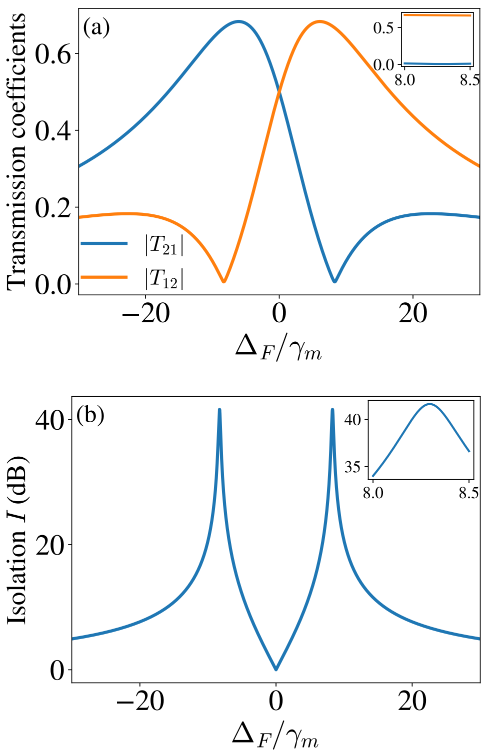

FIG. 2. (a) Transmission coefficients as a function of Δ_F/γ_m. (b) The isolation ratio as a function of Δ_F/γ_m. The parameters are $\Delta = 0$, $g_0/2\pi = 41\,\text{MHz}$, $G = 0.5$, $\kappa/2\pi = 1.1\,\text{MHz}$, $\gamma_m/2\pi = 4\,\text{MHz}$, $\eta = 0.5$, $P_1 = P_2 = P_3 = 100\,\text{mW}$, and $\omega_m/2\pi = 10.1\,\text{GHz}$, which are typical experimentally utilized parameters [25,66,73,74].

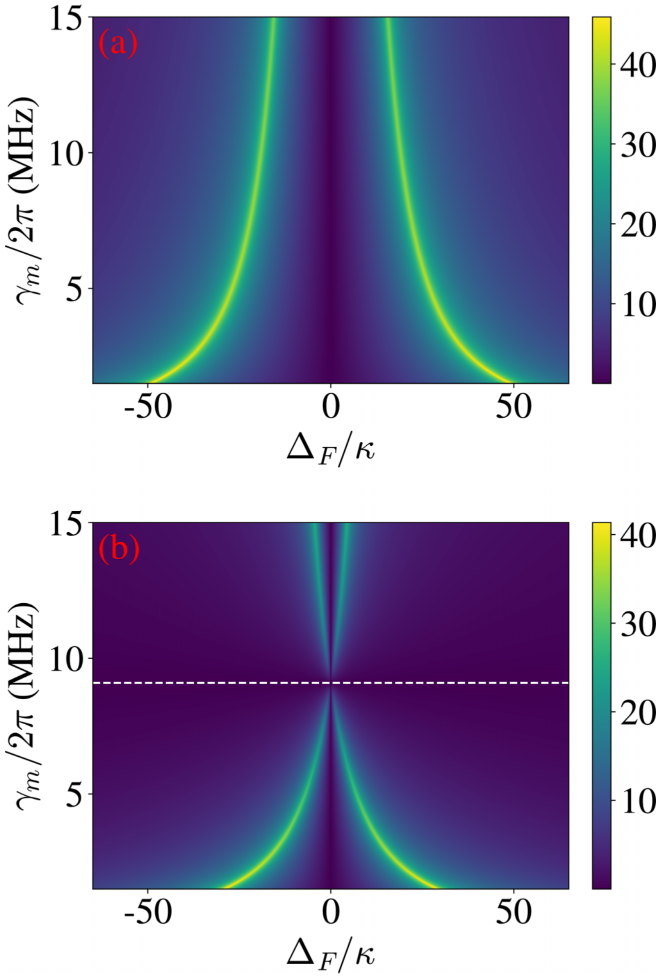

FIG. 3. The isolation ratio I vs Δ_F/κ and γ_m. $\Delta/\kappa = 0$ in panel (a) and 20 in panel (b). $\kappa/2\pi = 1.1$ MHz. The other parameters are the same as in Fig. 2. The plot is symmetric with respect to the line $\Delta_F/\kappa = 0$. The maximum values of I are 45.890 dB (when $\gamma_m = 1.5\,\text{MHz}$) in panel (a) and 41.352 dB (when $\gamma_m = 1.503\,\text{MHz}$) in panel (b).

cavity is not rotating, causing $\Delta_1 = \Delta_2$ and thus eliminating nonreciprocity.

We now turn our attention to investigating the impact of γ_m on the isolation ratio I. As can be seen from Fig. 3(a), for any given value of Δ_F, an optimal value of γ_m can always be found that maximizes the isolation ratio I. This maximum achievable I can be sustained at a high level of around 40 dB. In particular, $I = 0$ when $\Delta_F/\kappa = 0$, which corresponds to reciprocal transmission. Furthermore, the entire plot is symmetric about the axis $\Delta_F/\kappa = 0$. The region where $\Delta_F/\kappa > 0$ corresponds to the case $|A_{1,\text{out}}|^2 > |A_{2,\text{out}}|^2$, while the region where $\Delta_F/\kappa < 0$ corresponds to $|A_{1,\text{out}}|^2 < |A_{2,\text{out}}|^2$; this characteristic is also present in Fig. 2(a). If we reverse the rotational direction of the WGM cavity, the physical meaning of the regions on either side of the symmetry axis is also interchanged (i.e., the region where $\Delta_F/\kappa > 0$ then corresponds to $|A_{1,\text{out}}|^2 < |A_{2,\text{out}}|^2$ and $\Delta_F/\kappa < 0$ to $|A_{1,\text{out}}|^2 > |A_{2,\text{out}}|^2$). Therefore, we can reverse the direction of nonreciprocal transmission simply by reversing the WGM cavity's rotation.

When $\Delta/\kappa \neq 0$, as shown in Fig. 3(b), we surprisingly find that when the system satisfies the condition $\Delta = g\sqrt{\frac{\kappa}{\gamma_m}}$, termed the impedance matching condition [21,59], the isolation ratio I becomes zero, corresponding to the white dashed line in the figure. We define the γ_m value satisfying the impedance matching condition as the reciprocal point γ_0. As observed from Eqs. (13) and (14), the satisfaction of the reciprocity condition by the system parameters leads to $|A_{1,\text{out}}|^2 = |A_{2,\text{out}}|^2$, under which I remains identically zero. Furthermore, in contrast to the $\Delta/\kappa = 0$ situation, when $\gamma_m > \gamma_0$, the system exhibits a reversal in the direction of nonreciprocal transmission. Specifically, in the regions where $\Delta_F/\kappa > 0$ ($\Delta_F/\kappa < 0$) and $\gamma_m > \gamma_0$, we observe $|A_{1,\text{out}}|^2 < |A_{2,\text{out}}|^2$ ($|A_{1,\text{out}}|^2 > |A_{2,\text{out}}|^2$). Naturally, we can expect the system's response to κ to mirror its response to γ_m in many respects, as illustrated in Fig. 4. We can also define a κ-dependent reciprocal point κ_0 via the impedance-matching condition. In contrast to γ_m, a reversal of the nonreciprocal transmission direction occurs when $\kappa < \kappa_0$. Consequently, by analyzing Figs. 3 and 4, we can find the κ and γ_m values that yield the maximum isolation I for a given g. Importantly, this maximum I can remain at a large and stable value over a certain range of parameter variations.

Next, we further investigate the relationship between the isolation ratio and γ_m, as well as κ. Please note that to clearly illustrate the change in nonreciprocal transmission direction, the vertical axis in Fig. 5 does not adopt the definition from Eq. (16). Instead, we define $I' = 10\log_{10}\frac{|A_{1,\text{out}}|^2}{|A_{2,\text{out}}|^2}$.

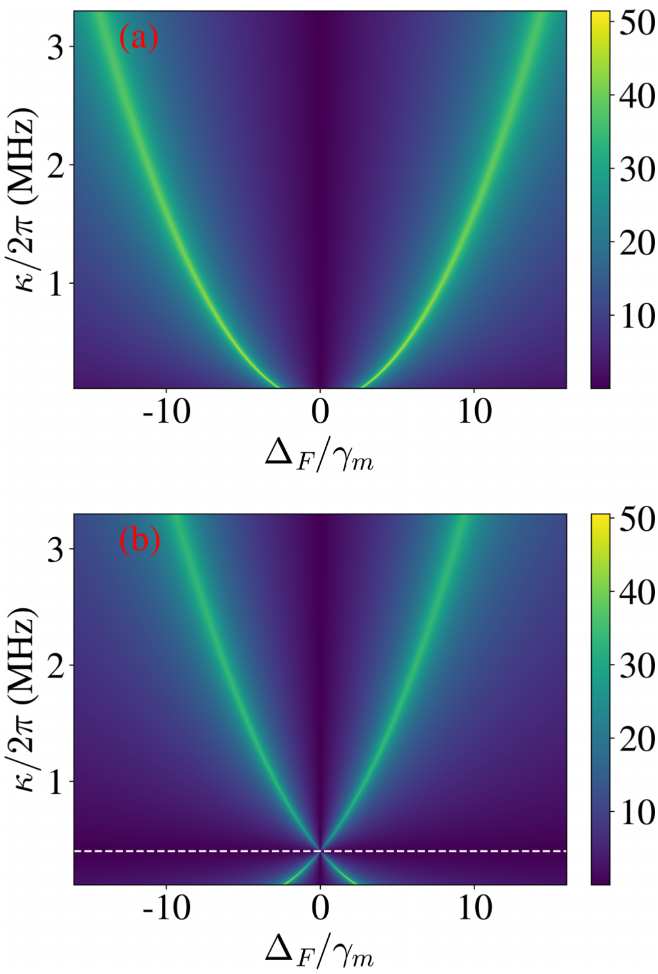

FIG. 4. The isolation ratio I vs Δ_F/γ_m and κ. $\Delta/\gamma_m = 0$ in panel (a) and 5 in panel (b). $\gamma_m/2\pi = 4$ MHz. The other parameters are the same as in Fig. 2. The maximum values of I are 51.437 dB (when $\kappa = 0.114$ MHz) in panel (a) and 50.542 dB (when $\kappa = 0.112$ MHz) in panel (b).

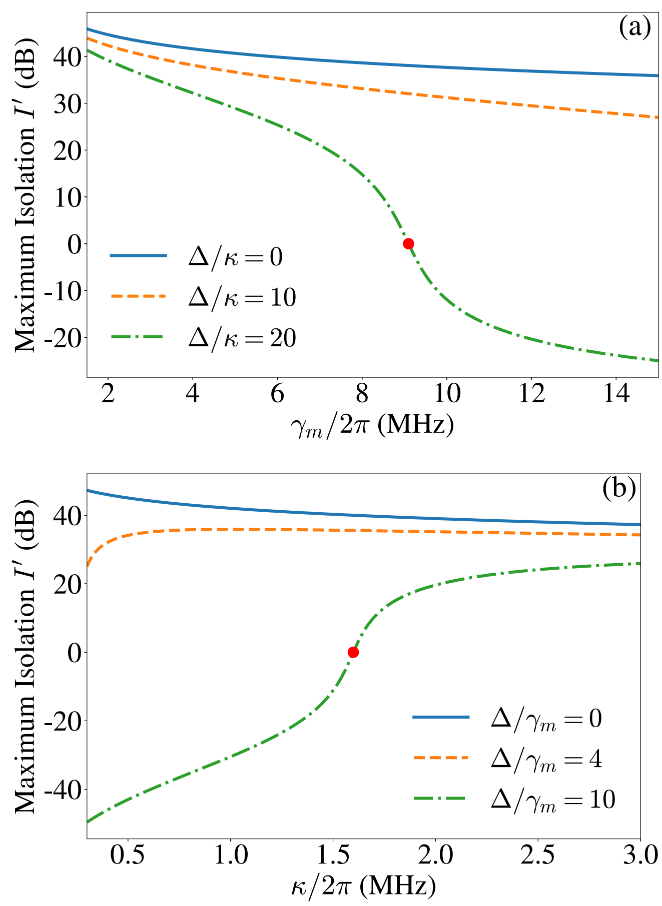

FIG. 5. Under optimal parameter Δ_F conditions, the isolation ratio I varies with (a) γ_m and (b) κ. $\kappa/2\pi = 1.1$ MHz in panel (a) and $\gamma_m/2\pi = 4$ MHz in panel (b). The other parameters are the same as in Fig. 2. The red dots represent the reciprocal points γ_0 and κ_0. Indeed, this functional plot corresponds to Eq. (18).

Consequently, when $I' < 0$, it signifies a reversal of the nonreciprocal transmission direction. As shown in Fig. 5, under the condition of optimal parameter Δ_F, the maximum achievable value of I' increases monotonically as either γ_m or κ decreases when $\Delta = 0$. For γ_m, this can be readily understood: A larger γ_m leads to stronger dissipation of the magnon mode, hindering efficient signal transmission and thus reducing I'. As for κ, a larger value enhances the escape efficiency of photons, which would increase the transmission coefficients. However, the forward transmission coefficient has already reached its maximum and remains almost unaffected by further increases in κ, resulting in a decrease in I'. Despite the increase in dissipation, we observe that I' exhibits minimal fluctuations and is stably maintained at a level exceeding 40 dB. This highlights the system's significant robustness to dissipation.

When $\Delta \neq 0$, in the regime where $\gamma_m < \gamma_0$, the maximum achievable I' exhibits a monotonic increase with decreasing γ_m, as depicted in Fig. 5(a). Nevertheless, when $\gamma_m > \gamma_0$, the system's nonreciprocal transmission direction reverses (i.e., $I' < 0$). Moreover, the absolute value of I' increases as γ_m increases. While this seems to contradict our earlier discussion, an examination of the system's transmission coefficients reveals a significant drop to very low values. For instance, at $\Delta/\kappa = 20$ and $\gamma_m/2\pi = 12$ MHz, we obtain $T_{21} = 0.0038$ and $T_{12} = 0.0004$. The extremely low transmission coefficients in this regime render information transmission nearly impossible. Furthermore, the forward transmission isolation decays rapidly as γ_m increases. Consider, for example, the cases where $\Delta/\kappa = 10$. When $\gamma_m/2\pi = 2$ MHz, $T_{21} = 0.0003$ and $T_{12} = 0.0382$. When $\gamma_m/2\pi = 4$ MHz, $T_{21} = 0.0002$ and $T_{12} = 0.0084$. The reason is that a larger Δ leads to a "dilute" of the nonreciprocity induced by the Sagnac effect, consequently weakening the nonreciprocal effect. On the other hand, detuning Δ makes it more difficult for the signal to couple into the optical cavity. Moreover, a larger γ_m prevents photons from the input port from effectively transferring to the output port via coupling with magnons. Both of these factors lead to a rapid decrease in transmission coefficients. This also compromises the system's robustness, making it more sensitive to dissipation. When γ_m increases, the forward transmission coefficient T_{12} exhibits greater sensitivity to γ_m compared to the reverse transmission coefficient T_{21}. Consequently, T_{12} decreases more rapidly until the impedance matching condition is satisfied. If γ_m is further increased, a

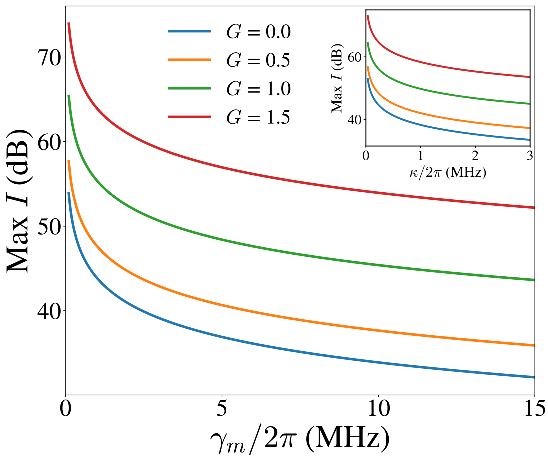

FIG. 6. The maximum isolation ratio I as a function of γ_m (main panel) and κ (inset) for different G values, under optimal Δ_F selection. $\kappa/2\pi = 1.1$ MHz in the main plot and $\gamma_m/2\pi = 4$ MHz in the inset. The other parameters are the same as in Fig. 2. The line colors used in the inset are consistent with the different G values presented in the main plot.

reversal of the nonreciprocal transmission will occur. Therefore, it is necessary to keep $\Delta = 0$ for practical parameter settings. The same analysis is applicable to κ. The sole distinction is that the regime of reversed nonreciprocal transmission and low transmission coefficients occurs when $\kappa < \kappa_0$, as illustrated in Fig. 5(b). In contrast to γ_m, a reduction in κ leads to a decrease in transmission coefficients. This is attributed to the fact that a smaller κ signifies a lower probability for photons to exit the cavity.

We now focus on investigating the impact of G on the nonreciprocal transmission efficiency of the system. Figure 6 shows the dependence of the maximum achievable isolation I on γ_m and κ for the optimal Δ_F. As illustrated in the main plot, there is a direct relationship where larger G values correspond to higher achievable I values, which lead to a significant enhancement in nonreciprocal transmission efficiency. For instance, with $G = 1$ and $\gamma_m/2\pi = 4$ MHz, I can exceed 50 dB, signifying almost perfect nonreciprocal transmission. Crucially, even with $G = 0$ (i.e., no squeeze applied), a substantial isolation ratio can still be obtained. This also shows that the system's nonreciprocity is independent of whether the magnon mode is squeezed. Similarly, the same conclusion holds for the analysis of κ, as depicted in the inset.

Since the previous discussion focused on a relatively specific situation $g_1' = g_2'$, it is essential to address a more general scenario here, such as $g_1' \neq g_2'$. At this point, Eq. (17) is no longer valid. The extremum points of R satisfy the following equation:

$$\Delta_{F_{1,2}} = \frac{1}{2}\left[U_1 \pm \sqrt{{U_1}^2 + U_2}\right], \quad U_1 = \sqrt{\frac{\kappa}{\gamma_m}}(g_1' - g_2'),$$
$$U_2 = \kappa^2 + 4\left(\Delta - g_1'\sqrt{\frac{\kappa}{\gamma_m}}\right)\left(\Delta - g_2'\sqrt{\frac{\kappa}{\gamma_m}}\right),$$
$$R(\Delta_{F_{1,2}}) = -\left(\frac{g_1'}{g_2'}\right)^2 \frac{\Delta - \Delta_{F_{1,2}} - g_2'\sqrt{\frac{\kappa}{\gamma_m}}}{\Delta + \Delta_{F_{1,2}} - g_1'\sqrt{\frac{\kappa}{\gamma_m}}}. \quad (19)$$

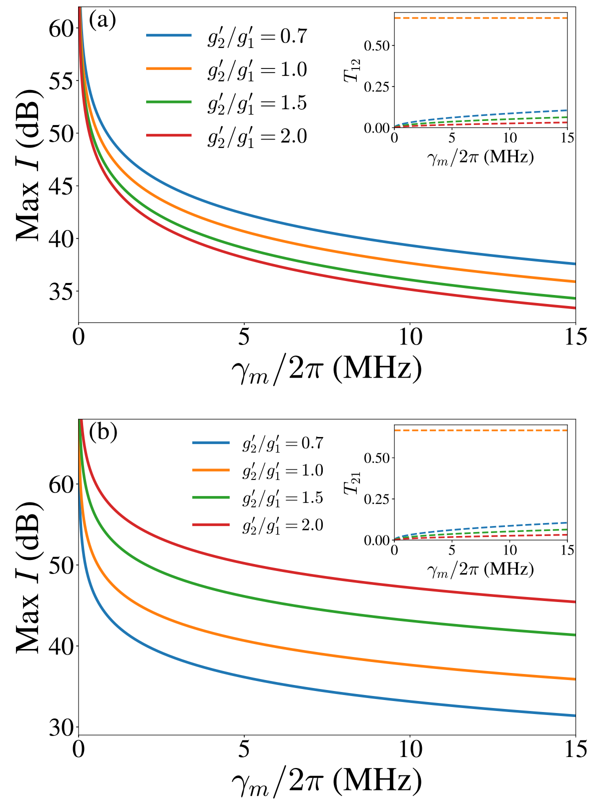

FIG. 7. The maximum achievable value of I at different g_2'/g_1' values varies with γ_m for (a) $\Delta_F > 0$ and (b) $\Delta_F < 0$. $\kappa/2\pi = 1.1$ MHz, $G = 0.5$, and $g_1/2\pi = 41$ MHz. The other parameters are the same as in Fig. 2. The insets in panels (a) and (b), respectively, show the variation of T_{12} and T_{21} with γ_m at the points where I reaches its maximum. The line colors used in the insets are consistent with the different g_2'/g_1' values presented in the main plot.

Under the condition $g_1' \neq g_2'$, it is usually the case that $\Delta_{F_1} \neq \Delta_{F_2}$. Consequently, the nonreciprocal transmission property, exhibiting symmetry around $\Delta_F = 0$, is broken. Perfectly symmetric reverse transmission efficiency cannot be achieved by simply reversing the WGM cavity's rotation. As depicted in Fig. 7(a), for $\Delta_F > 0$ (corresponding to $|A_{1,\mathrm{out}}|^2 > |A_{2,\mathrm{out}}|^2$), the maximum achievable I is plotted as a function of γ_m for various g_2'/g_1' ratios. It can be found that a smaller ratio of g_2'/g_1' leads to a higher forward transmission isolation. This observation is readily understood by analyzing the expression

$$R = \left|\frac{-ig_1' D_2 F_3 - g_1' g_2' F_2}{-ig_2' D_1 F_3 - g_1' g_2' F_1}\right|^2. \quad (20)$$

With g_1' held constant, a reduction in g_2' results in a larger R value, which consequently enhances the forward transmission isolation of the system. When $\Delta_F < 0$ (corresponding to $|A_{1,\mathrm{out}}|^2 < |A_{2,\mathrm{out}}|^2$), the situation is reversed, whereby an increase in g_2' enhances the system's reverse transmission isolation, a behavior demonstrated in Fig. 7(b). However, calculating the transmission coefficients reveals significant attenuation, as shown in the insets of Figs. 7(a) and 7(b). Moreover, this attenuation becomes more severe as the difference between g_1' and g_2' increases. For example, at $\Delta_F < 0$ and $\gamma_m/2\pi = 4$ MHz, T_{21} is 0.033 when $g_2'/g_1' = 1.5$, and

0.017 when $g_2'/g_1' = 2.0$. Therefore, it is necessary to maintain $g_1' = g_2'$ in practical parameter tuning. The analysis for γ_m is directly transferable to κ. For the sake of brevity, further discussion is omitted. Drawing from the preceding discussions, we see that with well-chosen system parameters, an isolation ratio exceeding 40 dB is easily attainable. This is a significant step toward realizing high-isolation nonreciprocal optical transmission systems.

IV. DISCUSSION AND CONCLUSIONS

Let us give a brief discussion of the feasibility of the experiment. The magnon frequency ω_m is experimentally controlled by tuning the external bias magnetic field H [75]. For a cavity-magnon system, a typical parameter choice is a cavity resonant frequency and magnon frequency of $\omega_0 = 193$ THz and $\omega_m = 10.1$ GHz [59–61,76–78]. The value $g_0 = 41$ MHz represents a typical cavity-magnon coupling strength employed in both experimental and numerical studies [35,36,73,79], and the squeezing parameter G typically ranges from 0 to 3 [71,72,80,81]. $\kappa/2\pi \sim 0.1$–100 MHz and γ_m is of the same order of magnitude [67,75,82–84]. For a rotating WGM cavity, typical parameter values can be taken as $n = 2.2$, $r = 1.1$ mm, and $\Omega/2\pi = 6.6$ kHz [66,85]. For this parameter set, Eq. (1) yields $\Delta_F \approx 65$ MHz, where we have considered only the first term because the other two are typically negligible. The magnitude of Δ_F is crucially limited by the fact that mechanical rotation angular velocity is typically below 10 kHz. Consequently, overcoming this limitation in the future would lead to a broader tunable parameter range.

In summary, we have theoretically proposed a scheme utilizing a cavity-magnon system to achieve ultrahigh nonreciprocal optical transmission through the exploitation of the Sagnac effect. In a rotating WGM cavity, the Fizeau shift induced by the Sagnac effect leads to nonreciprocal optical transmission. Our analysis demonstrates that, under experimentally feasible parameters, it is possible to attain nonreciprocal transmission with a high isolation ratio exceeding 40 dB, which also exhibits significant robustness against variations in angular velocity Ω and dissipation. Moreover, the optical isolation ratio can be further enhanced by increasing the squeezing parameter G. A notable feature of this system is the reconfigurability of the transmission direction, which can be readily reversed by simply changing the rotation direction of the resonator, without requiring any modifications to other system parameters. The proposed nonreciprocal optical transmission system offers several advantages, including a high isolation ratio, compact form factor, and operational simplicity. These attributes collectively make it a promising candidate for realizing on-chip optical isolators with enhanced signal-to-noise performance.

DATA AVAILABILITY

The data that support the findings of this article are not publicly available upon publication because it is not technically feasible and/or the cost of preparing, depositing, and hosting the data would be prohibitive within the terms of this research project. These data are available from the authors upon reasonable request.

[1] S. Barzanjeh, A. Xuereb, A. Alù, S. A. Mann, N. Nefedkin, V. Peano, and P. Rabl, Nonreciprocity in quantum technology, arXiv:2508.03945 [quant-ph].

[2] D. L. Sounas and A. Alù, Non-reciprocal photonics based on time modulation, Nat. Photon. **11**, 774 (2017).

[3] T. Shui, W.-X. Yang, M.-T. Cheng, and R.-K. Lee, Optical nonreciprocity and nonreciprocal photonic devices with directional four-wave mixing effect, Opt. Express **30**, 6284 (2022).

[4] H. Xie, L.-W. He, X. Shang, G.-W. Lin, and X.-M. Lin, Nonreciprocal photon blockade in cavity optomagnonics, Phys. Rev. A **106**, 053707 (2022).

[5] T. Mariz, J. R. Nascimento, and A. Petrov, *Lorentz Symmetry Breaking—Classical and Quantum Aspects*, SpringerBriefs in Physics (Springer, Cham, 2023).

[6] D. Jalas, A. Petrov, M. Eich, W. Freude, S. Fan, Z. Yu, R. Baets, M. Popović, A. Melloni, J. D. Joannopoulos *et al.*, What is—and what is not—an optical isolator, Nat. Photon. **7**, 579 (2013).

[7] K. L. Tsakmakidis, L. Shen, S. A. Schulz, X. Zheng, J. Upham, X. Deng, H. Altug, A. F. Vakakis, and R. W. Boyd, Breaking Lorentz reciprocity to overcome the time-bandwidth limit in physics and engineering, Science **356**, 1260 (2017).

[8] Z.-Y. Wang, J. Qian, Y.-P. Wang, J. Li, and J. Q. You, Realization of the unidirectional amplification in a cavity magnonic system, Appl. Phys. Lett. **123**, 153904 (2023).

[9] E. I. Rosenthal, B. J. Chapman, A. P. Higginbotham, J. Kerckhoff, and K. W. Lehnert, Breaking Lorentz reciprocity with frequency conversion and delay, Phys. Rev. Lett. **119**, 147703 (2017).

[10] L. J. Aplet and J. W. Carson, A Faraday effect optical isolator, Appl. Opt. **3**, 544 (1964).

[11] J. A. Haigh, S. Langenfeld, N. J. Lambert, J. J. Baumberg, A. J. Ramsay, A. Nunnenkamp, and A. J. Ferguson, Magneto-optical coupling in whispering-gallery-mode resonators, Phys. Rev. A **92**, 063845 (2015).

[12] C.-Z. Chai, H.-Q. Zhao, H. X. Tang, G.-C. Guo, C.-L. Zou, and C.-H. Dong, Non-reciprocity in high-Q ferromagnetic microspheres via photonic spin–orbit coupling, Laser Photon. Rev. **14**, 1900252 (2020).

[13] Z. Yu and S. Fan, Complete optical isolation created by indirect interband photonic transitions, Nat. Photon. **3**, 91 (2009).

[14] D.-W. Wang, H.-T. Zhou, M.-J. Guo, J.-X. Zhang, J. Evers, and S.-Y. Zhu, Optical diode made from a moving photonic crystal, Phys. Rev. Lett. **110**, 093901 (2013).

[15] R. Fleury, D. L. Sounas, C. F. Sieck, M. R. Haberman, and A. Alù, Sound isolation and giant linear nonreciprocity in a compact acoustic circulator, Science **343**, 516 (2014).

[16] F. Nazari, N. Bender, H. Ramezani, M. Moravvej-Farshi, D. N. Christodoulides, and T. Kottos, Optical isolation via pt-symmetric nonlinear Fano resonances, Opt. Express **22**, 9574 (2014).

[17] A. R. Hamann, C. Müller, M. Jerger, M. Zanner, J. Combes, M. Pletyukhov, M. Weides, T. M. Stace, and A. Fedorov, Nonreciprocity realized with quantum nonlinearity, Phys. Rev. Lett. **121**, 123601 (2018).
[18] L. Fan, J. Wang, L. T. Varghese, H. Shen, B. Niu, Y. Xuan, A. M. Weiner, and M. Qi, An all-silicon passive optical diode, Science **335**, 447 (2012).
[19] X.-W. Xu and Y. Li, Optical nonreciprocity and optomechanical circulator in three-mode optomechanical systems, Phys. Rev. A **91**, 053854 (2015).
[20] X.-B. Yan, H.-L. Lu, F. Gao, and L. Yang, Perfect optical nonreciprocity in a double-cavity optomechanical system, Front. Phys. **14**, 52601 (2019).
[21] X.-W. Xu, L. N. Song, Q. Zheng, Z. H. Wang, and Y. Li, Optomechanically induced nonreciprocity in a three-mode optomechanical system, Phys. Rev. A **98**, 063845 (2018).
[22] Z. Shen, Y.-L. Zhang, Y. Chen, C.-L. Zou, Y.-F. Xiao, X.-B. Zou, F.-W. Sun, G.-C. Guo, and C.-H. Dong, Experimental realization of optomechanically induced non-reciprocity, Nat. Photon. **10**, 657 (2016).
[23] Z. Shen, Y.-L. Zhang, Y. Chen, F.-W. Sun, X.-B. Zou, G.-C. Guo, C.-L. Zou, and C.-H. Dong, Reconfigurable optomechanical circulator and directional amplifier, Nat. Commun. **9**, 1797 (2018).
[24] Q.-S. Tan, Y.-F. Jiao, Y. Zuo, L. Xu, J.-Q. Liao, and L.-M. Kuang, Reinforcement-learning-assisted nonreciprocal optomechanical gyroscope, Phys. Rev. A **111**, 063504 (2025).
[25] B. Zare Rameshti, S. Viola Kusminskiy, J. A. Haigh, K. Usami, D. Lachance-Quirion, Y. Nakamura, C.-M. Hu, H. X. Tang, G. E. Bauer, and Y. M. Blanter, Cavity magnonics, Phys. Rep. **979**, 1 (2022).
[26] H. Yuan, Y. Cao, A. Kamra, R. A. Duine, and P. Yan, Quantum magnonics: When magnon spintronics meets quantum information science, Phys. Rep. **965**, 1 (2022).
[27] M. Collet, X. De Milly, O. d'Allivy Kelly, V. V. Naletov, R. Bernard, P. Bortolotti, J. Ben Youssef, V. Demidov, S. Demokritov, J. L. Prieto *et al.*, Generation of coherent spin-wave modes in yttrium iron garnet microdiscs by spin–orbit torque, Nat. Commun. **7**, 10377 (2016).
[28] H. Y. Yuan and M.-H. Yung, Thermodynamic entanglement of magnonic condensates, Phys. Rev. B **97**, 060405 (2018).
[29] T. Morimae, A. Sugita, and A. Shimizu, Macroscopic entanglement of many-magnon states, Phys. Rev. A **71**, 032317 (2005).
[30] D. Zhang, X.-M. Wang, T.-F. Li, X.-Q. Luo, W. Wu, F. Nori, and J. You, Cavity quantum electrodynamics with ferromagnetic magnons in a small yttrium-iron-garnet sphere, npj Quantum Inf. **1**, 15014 (2015).
[31] L. Chen, Y. Liu, L. Bin, S.-Y. Ye, and Z.-R. Zhong, Simultaneous cooling of the internal and external degrees of freedom of a levitated micromagnet in a cavity magnomechanical system, Phys. Rev. Res. **7**, 033157 (2025).
[32] X. Deng, K.-K. Zhang, T. Shui, and W.-X. Yang, Nonreciprocal unconventional magnon blockade via the Sagnac-Fizeau shift in an optomagnonic system, Phys. Rev. A **110**, 063711 (2024).
[33] H. Zhang, C. Wang, Q. Bao, Z. Liu, H. Liu, and J.-J. Xiao, Topological mode switch by exceptional point encircling in a cavity magnonic system, Opt. Lett. **50**, 4154 (2025).
[34] Y.-P. Wang, G.-Q. Zhang, D. Zhang, X.-Q. Luo, W. Xiong, S.-P. Wang, T.-F. Li, C.-M. Hu, and J. Q. You, Magnon Kerr effect in a strongly coupled cavity-magnon system, Phys. Rev. B **94**, 224410 (2016).
[35] G. Zhang, Y. Wang, and J. You, Theory of the magnon Kerr effect in cavity magnonics, Sci. China Math. **62**, 987511 (2019).
[36] Y.-P. Wang, G.-Q. Zhang, D. Zhang, T.-F. Li, C.-M. Hu, and J. Q. You, Bistability of cavity magnon polaritons, Phys. Rev. Lett. **120**, 057202 (2018).
[37] D. Zhang, X.-Q. Luo, Y.-P. Wang, T.-F. Li, and J. You, Observation of the exceptional point in cavity magnon-polaritons, Nat. Commun. **8**, 1368 (2017).
[38] Y. Cao, P. Yan, H. Huebl, S. T. B. Goennenwein, and G. E. W. Bauer, Exchange magnon-polaritons in microwave cavities, Phys. Rev. B **91**, 094423 (2015).
[39] L. Bai, M. Harder, P. Hyde, Z. Zhang, C.-M. Hu, Y. P. Chen, and J. Q. Xiao, Cavity mediated manipulation of distant spin currents using a cavity-magnon-polariton, Phys. Rev. Lett. **118**, 217201 (2017).
[40] P. Hyde, B. M. Yao, Y. S. Gui, G.-Q. Zhang, J. Q. You, and C.-M. Hu, Direct measurement of foldover in cavity magnon-polariton systems, Phys. Rev. B **98**, 174423 (2018).
[41] G.-Q. Zhang and J. Q. You, Higher-order exceptional point in a cavity magnonics system, Phys. Rev. B **99**, 054404 (2019).
[42] T.-X. Lu, H. Zhang, Q. Zhang, and H. Jing, Exceptional-point-engineered cavity magnomechanics, Phys. Rev. A **103**, 063708 (2021).
[43] Y. Tabuchi, S. Ishino, T. Ishikawa, R. Yamazaki, K. Usami, and Y. Nakamura, Hybridizing ferromagnetic magnons and microwave photons in the quantum limit, Phys. Rev. Lett. **113**, 083603 (2014).
[44] Y. Tabuchi, S. Ishino, A. Noguchi, T. Ishikawa, R. Yamazaki, K. Usami, and Y. Nakamura, Coherent coupling between a ferromagnetic magnon and a superconducting qubit, Science **349**, 405 (2015).
[45] O. O. Soykal and M. E. Flatté, Strong field interactions between a nanomagnet and a photonic cavity, Phys. Rev. Lett. **104**, 077202 (2010).
[46] X. Zhang, C.-L. Zou, L. Jiang, and H. X. Tang, Strongly coupled magnons and cavity microwave photons, Phys. Rev. Lett. **113**, 156401 (2014).
[47] J. Bourhill, N. Kostylev, M. Goryachev, D. L. Creedon, and M. E. Tobar, Ultrahigh cooperativity interactions between magnons and resonant photons in a YIG sphere, Phys. Rev. B **93**, 144420 (2016).
[48] M. Harder, Y. Yang, B. M. Yao, C. H. Yu, J. W. Rao, Y. S. Gui, R. L. Stamps, and C.-M. Hu, Level attraction due to dissipative magnon-photon coupling, Phys. Rev. Lett. **121**, 137203 (2018).
[49] B. Yao, Y. Gui, J. Rao, S. Kaur, X. Chen, W. Lu, Y. Xiao, H. Guo, K.-P. Marzlin, and C.-M. Hu, Cooperative polariton dynamics in feedback-coupled cavities, Nat. Commun. **8**, 1437 (2017).
[50] D. Lachance-Quirion, Y. Tabuchi, A. Gloppe, K. Usami, and Y. Nakamura, Hybrid quantum systems based on magnonics, Appl. Phys. Express **12**, 070101 (2019).
[51] Q.-K. Wan, H.-L. Shi, and X.-W. Guan, Quantum-enhanced metrology in cavity magnonics, Phys. Rev. B **109**, L041301 (2024).
[52] G. Flower, M. Goryachev, J. Bourhill, and M. E. Tobar, Experimental implementations of cavity-magnon systems: From ultra strong coupling to applications in precision measurement, New J. Phys. **21**, 095004 (2019).

[53] Q. Cai, J. Liao, B. Shen, G. Guo, and Q. Zhou, Microwave quantum illumination via cavity magnonics, Phys. Rev. A **103**, 052419 (2021).
[54] A. Osada, R. Hisatomi, A. Noguchi, Y. Tabuchi, R. Yamazaki, K. Usami, M. Sadgrove, R. Yalla, M. Nomura, and Y. Nakamura, Cavity optomagnonics with spin-orbit coupled photons, Phys. Rev. Lett. **116**, 223601 (2016).
[55] J. A. Haigh, A. Nunnenkamp, A. J. Ramsay, and A. J. Ferguson, Triple-resonant Brillouin light scattering in magneto-optical cavities, Phys. Rev. Lett. **117**, 133602 (2016).
[56] R. Hisatomi, A. Osada, Y. Tabuchi, T. Ishikawa, A. Noguchi, R. Yamazaki, K. Usami, and Y. Nakamura, Bidirectional conversion between microwave and light via ferromagnetic magnons, Phys. Rev. B **93**, 174427 (2016).
[57] X. Zhang, C.-L. Zou, N. Zhu, F. Marquardt, L. Jiang, and H. X. Tang, Magnon dark modes and gradient memory, Nat. Commun. **6**, 8914 (2015).
[58] R.-C. Shen, Y.-P. Wang, J. Li, S.-Y. Zhu, G. S. Agarwal, and J. Q. You, Long-time memory and ternary logic gate using a multistable cavity magnonic system, Phys. Rev. Lett. **127**, 183202 (2021).
[59] C. Kong, H. Xiong, and Y. Wu, Magnon-induced nonreciprocity based on the magnon Kerr effect, Phys. Rev. Appl. **12**, 034001 (2019).
[60] Y.-L. Ren, S.-L. Ma, J.-K. Xie, X.-K. Li, and F.-L. Li, Nonreciprocal optical transmission in cavity optomagnonics, Opt. Express **29**, 41399 (2021).
[61] C. Kong, X.-M. Bao, J.-B. Liu, and H. Xiong, Magnon-mediated nonreciprocal microwave transmission based on quantum interference, Opt. Express **29**, 25477 (2021).
[62] Y.-P. Wang, J. W. Rao, Y. Yang, P.-C. Xu, Y. S. Gui, B. M. Yao, J. Q. You, and C.-M. Hu, Nonreciprocity and unidirectional invisibility in cavity magnonics, Phys. Rev. Lett. **123**, 127202 (2019).
[63] Y. Ming and R.-C. Yang, Nonreciprocal transmission, reflection, and absorption in non-Hermitian cavity magnonics, Results Phys. **64**, 107915 (2024).
[64] Y.-J. Xu, L.-H. Zhai, P. Fu, S.-J. Cheng, and G.-Q. Zhang, Nonreciprocal quantum phase transition in cavity magnonics, Phys. Rev. A **110**, 043704 (2024).
[65] H. Xie, L.-W. He, C.-G. Liao, Z.-H. Chen, and X.-M. Lin, Generation of robust optical entanglement in cavity optomagnonics, Opt. Express **31**, 7994 (2023).
[66] S. Maayani, R. Dahan, Y. Kligerman, E. Moses, A. U. Hassan, H. Jing, F. Nori, D. N. Christodoulides, and T. Carmon, Flying couplers above spinning resonators generate irreversible refraction, Nature (London) **558**, 569 (2018).
[67] M. Aspelmeyer, T. J. Kippenberg, and F. Marquardt, Cavity optomechanics, Rev. Mod. Phys. **86**, 1391 (2014).
[68] J. Li, S.-Y. Zhu, and G. S. Agarwal, Squeezed states of magnons and phonons in cavity magnomechanics, Phys. Rev. A **99**, 021801 (2019).
[69] Q. Guo, J. Cheng, H. Tan, and J. Li, Magnon squeezing by two-tone driving of a qubit in cavity-magnon-qubit systems, Phys. Rev. A **108**, 063703 (2023).
[70] M.-S. Ding, L. Zheng, Y. Shi, and Y.-J. Liu, Magnon squeezing enhanced entanglement in a cavity magnomechanical system, J. Opt. Soc. Am. B **39**, 2665 (2022).
[71] A.-B. Xia, J. Cheng, D.-L. Tian, C.-J. Han, and Y. P. Wang, Magnon squeezing induced by virtual photons in a magnon-cavity-qubit system, Phys. Rev. A **111**, 053707 (2025).
[72] W. Qin, V. Macrì, A. Miranowicz, S. Savasta, and F. Nori, Emission of photon pairs by mechanical stimulation of the squeezed vacuum, Phys. Rev. A **100**, 062501 (2019).
[73] Z. Zhang, M. O. Scully, and G. S. Agarwal, Quantum entanglement between two magnon modes via Kerr nonlinearity driven far from equilibrium, Phys. Rev. Res. **1**, 023021 (2019).
[74] G. C. Righini, Y. Dumeige, P. Féron, M. Ferrari, G. Nunzi Conti, D. Ristic, and S. Soria, Whispering gallery mode microresonators: Fundamentals and applications, Riv. Nuovo Cimento **34**, 435 (2011).
[75] X. Zhang, C.-L. Zou, L. Jiang, and H. X. Tang, Cavity magnomechanics, Sci. Adv. **2**, e1501286 (2016).
[76] A. Osada, A. Gloppe, R. Hisatomi, A. Noguchi, R. Yamazaki, M. Nomura, Y. Nakamura, and K. Usami, Brillouin light scattering by magnetic quasivortices in cavity optomagnonics, Phys. Rev. Lett. **120**, 133602 (2018).
[77] X. Zhang, N. Zhu, C.-L. Zou, and H. X. Tang, Optomagnonic whispering gallery microresonators, Phys. Rev. Lett. **117**, 123605 (2016).
[78] S. Barzanjeh, S. Guha, C. Weedbrook, D. Vitali, J. H. Shapiro, and S. Pirandola, Microwave quantum illumination, Phys. Rev. Lett. **114**, 080503 (2015).
[79] J. Yao, C. Lu, X. Fan, D. Xue, G. E. Bridges, and C.-M. Hu, Nonreciprocal control of the speed of light using cavity magnonics, Phys. Rev. Lett. **134**, 196904 (2025).
[80] Z.-B. Yang, H. Jin, J.-W. Jin, J.-Y. Liu, H.-Y. Liu, and R.-C. Yang, Bistability of squeezing and entanglement in cavity magnonics, Phys. Rev. Res. **3**, 023126 (2021).
[81] J.-X. Wang, Q. Guo, Y. Zhang, G. Li, and T. Zhang, Steady-squeezed-state generation via Kerr nonlinearity in cavity magnonics system, J. Phys. A: Math. Theor. **58**, 235302 (2025).
[82] F. H. Mathkoor, S. Singh, R. Ahmed, J.-X. Peng, M. Amazioug, M. Khalid, and A. Sohail, Bipartite entanglement and Gaussian quantum steering in a whispering gallery mode coupled with two magnon modes, Sci. Rep. **15**, 13503 (2025).
[83] S. Sharma, Y. M. Blanter, and G. E. W. Bauer, Optical cooling of magnons, Phys. Rev. Lett. **121**, 087205 (2018).
[84] J. Chen, X.-G. Fan, W. Xiong, D. Wang, and L. Ye, Nonreciprocal photon-phonon entanglement in Kerr-modified spinning cavity magnomechanics, Phys. Rev. A **109**, 043512 (2024).
[85] Q. Zheng, W. Zhong, G. Cheng, and A. Chen, Nonreciprocal microwave-optical entanglement in a magnon-based hybrid system, J. Appl. Phys. **135**, 084401 (2024).